Study of Aerosol/Cloud/Radiation Interactions Over the Atmospheric Radiation Measurement Program Southern Great Plain Site

C. Chuang and S. Chin
Lawrence Livermore National Laboratory
Livermore, California

Introduction

While considerable advances in the understanding of atmospheric processes and feedbacks in the climate system have led to a better representation of these mechanisms in general circulation models, the greatest uncertainty in predictability of future climate arises from clouds and their interactions with radiation. To explore this uncertainty, the cloud resolving model has evolved as one of the main tools for understanding and testing cloud feedback processes in climate models, whereas the indirect effects of aerosols are closely linked with cloud feedback processes. In this study, we incorporated an existing parameterization of cloud drop concentration (Chuang et al. 2002a) with aerosol prediction from a global chemistry/aerosol model (IMPACT) (Rotman et al. 2004; Chuang et al. 2002b; Chuang et al. 2005) into the Lawrence Livermore National Laboratory (LLNL) cloud resolving model (Chin 1994; Chin et al. 1995; Chin and Wilhelmson 1998). This was done to investigate the effects of aerosols on cloud/precipitation properties and the resulting radiation fields over the Southern Great Plains (SGP) site.

Our first focus on this aspect is to compare the simulated aerosol properties to the Atmospheric Radiation Measurement (ARM) Program measurements. Figure 1 presents the calculated aerosol optical depth (AOD) at 355 nm using National Center for Atmospheric Research CAM3 (general circulation model output at 1°×1.25°, 26 layers) and NASA GEOS3 2001 (assimilated data at 1°× 1°, 48 layers) meteorology over SGP site together with those from the ground-based Raman lidar (Ferrare et al. 2001). The simulated seasonality of AOD using CAM3, in general, agrees with measurements though the magnitude is slightly lower. On the contrary, simulated AOD using GEOS3 shows a very different pattern from measurements. The nonlinear dependence of AOD on relative humidity diagnosed from large-scale variables may be a possible explanation since the simulated aerosol burdens alone cannot explain for the discrepancy. To explore this issue further, we present in Figure 2 the simulated aerosol column burden as well as the "derived" AOD over the SGP site as a function of relative humidity. We found that the "derived" AOD from aerosol burden using GEOS3 has a much better agreement with
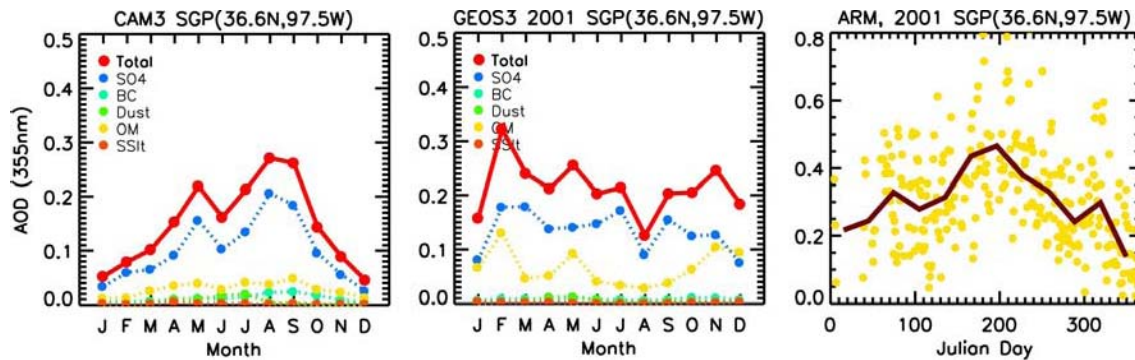
Figure 1. Simulated seasonal variations of aerosol optical depth at 355 nm over the SGP site using CAM3 (left) and GEOS3 2001 (middle) meteorology. Also shown are the measurements from Raman lidar (right) with scattered circle for daily average and solid curve for monthly average.
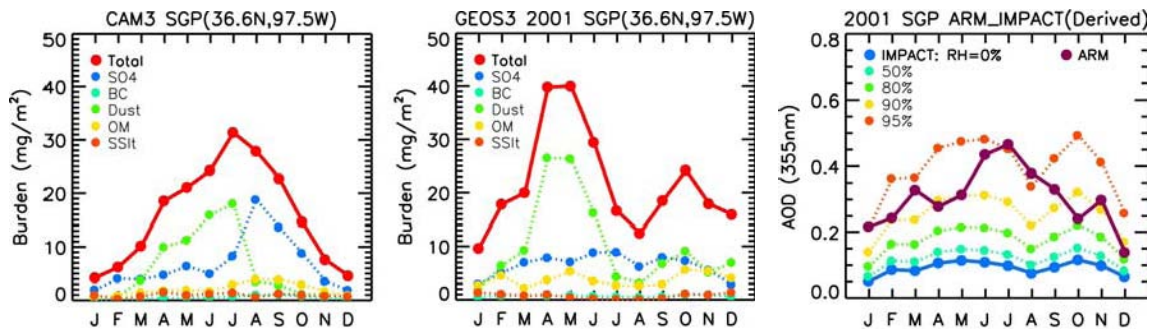

Figure 2. Simulated seasonal variations of column burden of aerosols over the SGP site using CAM3 (left) and GEOS3 2001 (middle) meteorology. Also shown on the right are the ARM data and the "derived" AOD as a function of relative humidity from the aerosol burden simulated with GEOS3 2001.

measurements when relative humidity = 95%. This does not imply that the relative humidity at the SGP site should be 95% all year; instead, it demonstrates the important role of relative humidity in the comparison of model simulations and measurements.

The simulated aerosol concentrations and components over the SGP site are incorporated into the two-dimensional version of the LLNL non-hydrostatic, fully compressible cloud resolving model to study the impacts of aerosols on the optical and microphysical characteristics of clouds. In this study, the cloud model simulates a squall-like precipitation system passing through the SGP site's Central Facility on June 19, 2004 (Figures 3a–d). Model framework is set up with varied horizontal (2 km in the central 900-km area with 50 stretching grids on both sides) and vertical resolution (50 m near the ground and gradually increased to 600 m at 3.3 km) with top layer at 20.7 km. The initial condition at 1400 Universal Time Coordinates (i.e., 9 A.M.) is modified from the 1130 Universal Time Coordinates sounding at the Central Facility as shown in Figure 3e. Though the convective available potential energy, 620 m^2s^{-2}, is small in this case, the treatment of prognostic surface energy is able to destabilize and moisten the environment near the ground and leads to the development of a squall-like precipitation system with substantial wind shear in the lowest 3 km. The vertical profiles of natural (SO4b, OCn,

submicron dust, and sea salt) and anthropogenic (SO4a, OC, and BC) aerosols applied into cloud resolving model are those monthly averages for June and are shown in Figure 4a, while the interrelationship between anthropogenic sulfate, aerosol number, updraft velocity, and liquid cloud nucleation described by Chuang et al. (2002a) is given in Figure 4b.
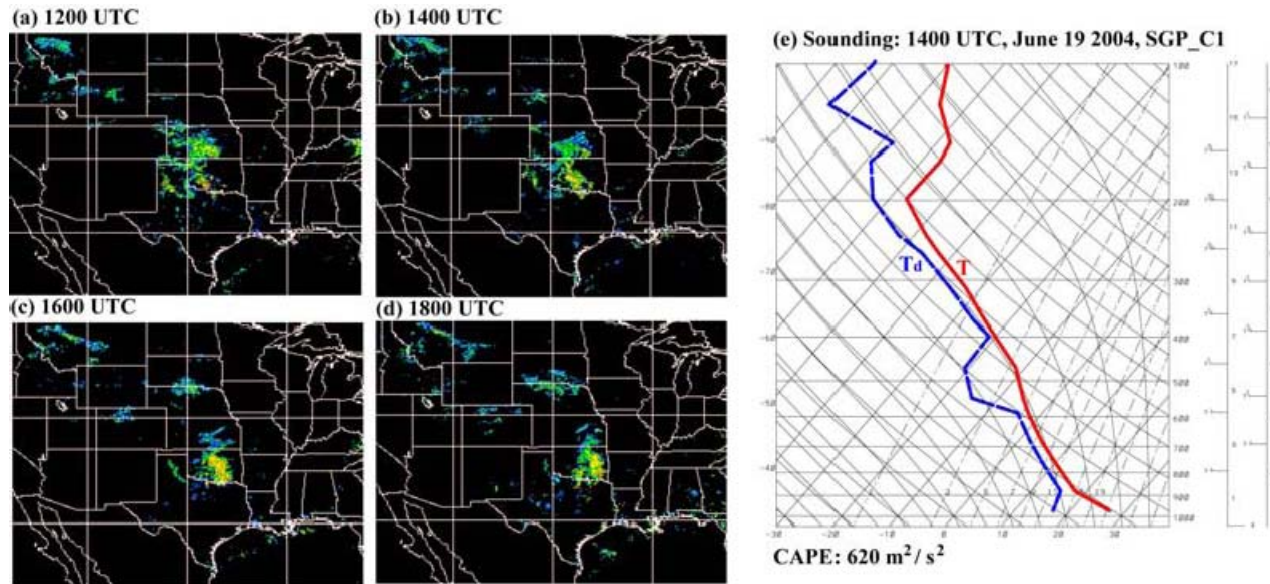

Figure 3. (a) - (d) Radar reflectivity of the selected precipitation system passing through the Central Facility of the SGP site on June 19, 2004. (e) Initial sounding. The horizontal velocity shown on the right is the normal-line component of winds, parallel to the propagation of rain band.
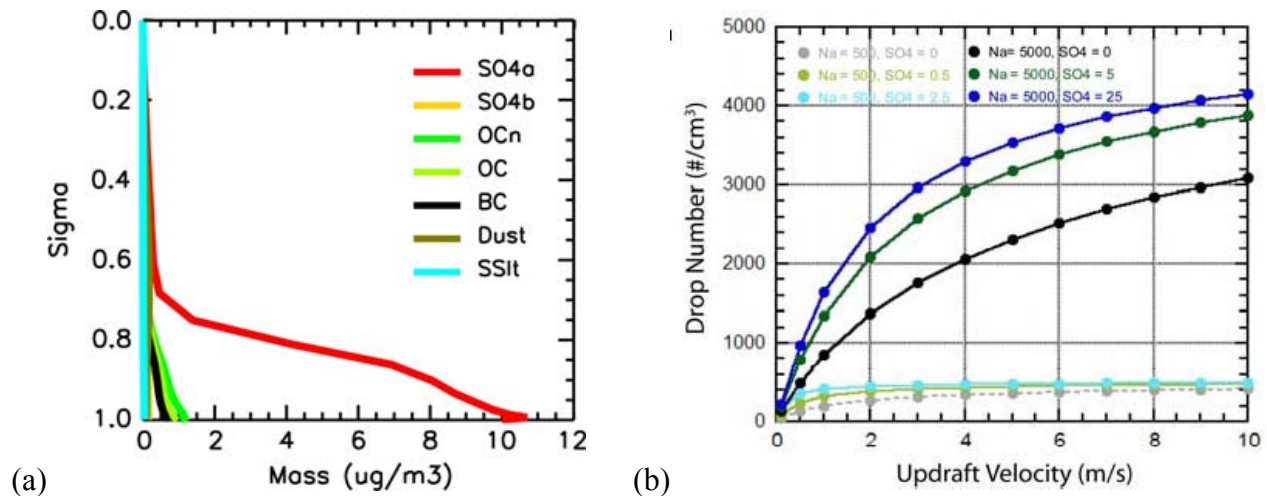

Figure 4. (a) Simulated vertical profiles of aerosol concentrations and components over the SGP site for June. (b) Variations of the predicted drop number concentrations with aerosol number, anthropogenic sulfate, and updraft velocity.

We examine how increases in cloud optical depth associated with aerosols impact shortwave (SW) and longwave (LW) radiative fluxes. We also study in detail the response of cloud microphysics to different aerosol characteristics. Additionally, we investigate the sensitivity of surface precipitation rate to different parameterizations of autoconversion (the process of forming raindrops by collisions and coalescence of cloud drops). Table 1 lists the experiments carried in this study. Four different parameterizations for autoconversion process are shown in the following.

Kessler (1969):
$$P_{Raut}\,(\text{s}^{-1}) = k\left(l_{cw} - l_{cwc}\right)$$
Eq. (1)

Berry (1968):
$$P_{Raut}\,(\text{s}^{-1}) = \frac{\rho\, l_{cw}^2}{1.2 \times 10^{-4} + \dfrac{1.569 \times 10^{-12}\, N_d}{D_o\, \rho\, l_{cw}}}$$
Eq. (2)

Beheng (1994):
$$P_{Raut}\,(\text{s}^{-1}) = \frac{6 \times 10^{25}\, n^{-1.7}\, N_d^{-3.3}\, (\rho\, l_{cw})^{4.7}}{\rho}$$
Eq. (3)

Chen and Cotton (1987):
$$P_{Raut}\,(\text{s}^{-1}) = C\, \frac{\rho}{\rho_w}\, l_{cw}^2 \left(\frac{\rho}{\rho_w}\, l_{cw}\, N_d\right)^{\frac{1}{3}} H\left(r_{vl} - r_{vlc}\right)$$
Eq. (4)

Table 1. List of physics processes used in sensitivity experiments.

Physics/Experiment	Control	1	2	3	4	5	6
Autoconversion	Kessler	Berry	Berry	Beheng	Beheng	Chen & Cotton	Chen & Cotton
Aerosols	N/A[1]	Natural	N + A[2]	Natural	N + A	Natural	N + A
Cloud Drops	Fixed	Predicted	Predicted	Predicted	Predicted	Predicted	Predicted
[1] N/A: Not Applied							
[2] N + A: Natural + Anthropogenic							

The control simulation prescribes the effective radius of liquid cloud droplet and does not explicitly account for aerosol effect on clouds. Other experiments apply cloud drop parameterization and predict the temporal and spatial variations of drop effective radius and concentration. Although processes associated with ice cloud remain unchanged in all experiments, it is possible that the properties of ice cloud can be influenced through processes between liquid and ice phases. Additionally, an identical threshold value of cloud water mixing ratio (l_{cwc} = 1 g kg^{-1}) is applied to these four autoconversion parameterizations even though individual scheme may have its own optimal value for different application.

(a) Effects of Aerosols on Cloud Optical Properties

The optical depth of liquid cloud is calculated as follows:

$$\tau_l = \sum_{k=1}^{K} \Delta h_k \ w_{L,k} \left[a_l^i + \frac{b_l^i}{r_{el}} \right]$$

Eq. (5)

where the index k represents cloud layer, Δh_k is the thickness of each cloud layer, wL,k is the cloud liquid water content. The spectral intervals (denoted by the superscript i) and coefficients are defined in Fu and Liou (1993). We examine how increases in cloud optical depth associated with aerosols impact SW and LW radiative fluxes at the top of model layer. As shown in Figure 5, anthropogenic aerosols enhance cloud optical depth through the reduction of r_{el} and result in a larger reflected SW flux. The so-called first indirect effect (or Twomey effect), where an increase in aerosols causes an increase in drop concentration and a decrease in drop size for fixed liquid water content, is clearly demonstrated during the first 5 hours when the predicted liquid and ice water content with or without anthropogenic aerosols are similar. Our results suggest that the enhancement of reflected SW by anthropogenic aerosols can be up to $17 - 20$ Wm^{-2} (averaged over the area of 200×1 km^2).

In Fu and Liou (1993), r_{el} is prescribed in a range between 4 and 31 μm, based on cloud types. To explore the sensitivity of reflected SW flux to the treatment of effective drop size, we compare experiments with predicted r_{el} to control simulation. We found that for $r_{el} = 5$ μm (a typical value used for continental cloud in general circulation models) the control simulation reflects a higher SW flux by about 30 Wm^{-2} than experiments 2, 4 and 6. This not only indicates the importance of aerosol/cloud interactions but also suggests a potential uncertainty associated with cloud/ radiation treatments in GCMs.

Contrary to the dependence of reflected SW flux on effective drop size, the outgoing LW flux is mainly determined by the altitude of clouds. Lower clouds trap outgoing LW flux from earth's surface more effectively and re-emit LW radiation at higher temperature than higher clouds. Since cloud structures are similar with or without anthropogenic aerosols before the first 5 hours, there is little difference in outgoing LW during this period. Afterwards, the evolution of convection development exhibits a strong dependence on aerosol concentration as well as the parameterization of autoconversion process, resulting in considerable variations in cloud structure and the outgoing LW flux.
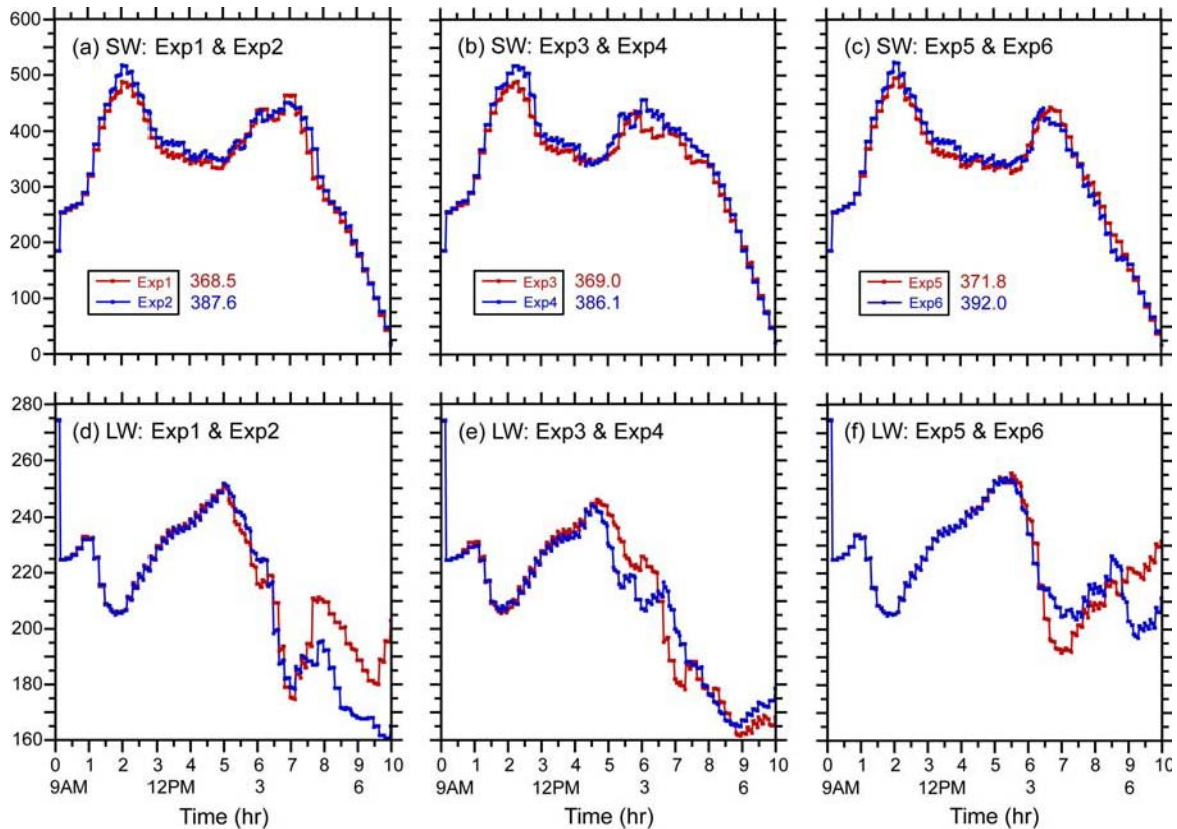
Figure 5. Averaged SW and LW fluxes (Wm^{-2}) at the top of the model layer over a domain of 200 km × 1 km with the convective core as the center. Also shown in the SW plots are the temporal averages between 10 a.m. and 2 p.m.

(b) Effects of Aerosols on Surface Precipitation Rate

Aerosols not only influence the optical properties of clouds but also tend to alter the cloud lifetime and precipitation efficiency through the reduction in drop size (the second indirect effect). Climate models that have attempted to quantify the effect of aerosols on clouds have shown that the magnitude of the second indirect effect is extremely sensitive to the parameterizations of autoconversion and cloud cover in the models (Lohmann and Feichter 1997). It is not yet clear whether these processes and the changes in these processes associated with aerosols is accurately described by the parameterizations currently in the models. To examine the sensitivity of the surface precipitation rate to the parameterization of autoconversion, we perform experiments with different representation of autoconversion and explore the response of convective cloud system to different aerosol concentrations. The first autoconversion scheme is from Berry (1968), the second one is from Beheng (1994) that has been applied into ECHAM general circulation model, and whereas the third one is based on Chen and Cotton (1987) employed in National Center for Atmospheric Research CAM2.

Figure 6 presents the time evolution of surface precipitation pattern using different parameterizations of autoconversion with and without anthropogenic aerosols. As demonstrated in the figures, once the initial convection triggered by the warm and moist bubble decays, the simulated cold cool is strong enough to interact with ambient wind shear to form a new convection after about $4-5$ hours. Conversely, the time-varying surface energy evolves an unfavorable condition for the development of new convection in the late afternoon. The time lag to trigger a new convection by cold pool as well as the duration and precipitation associated with the active convective band vary with the representation of autoconversion and aerosol concentration. For Berry and Chen & Cotton schemes, the patterns of surface precipitation rate are similar with or without anthropogenic aerosols but the duration of precipitation with higher aerosol concentration is somewhat longer. In contrast, considerable differences in the evolution of surface precipitation pattern are noticed for Beheng scheme.
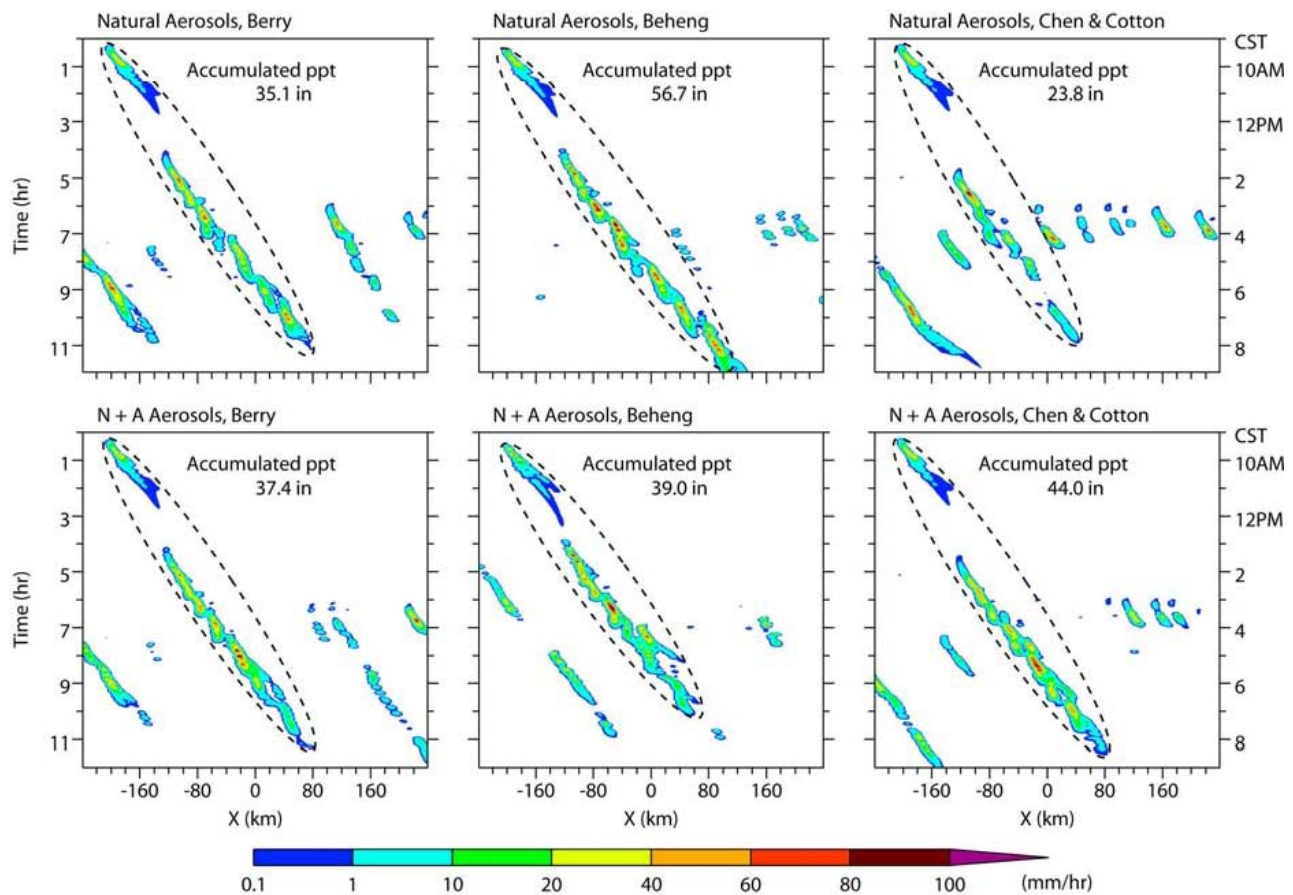

Figure 6. Simulated surface precipitation rate (mm/hr) using different schemes of autoconversion with and without anthropogenic aerosols. Also shown is the accumulated precipitation associated with the active convective band (denoted by the dashed curve).

We are in the process to examine whether ARM data can be used to verify the response of the cloud resolving model and then explore the potential of ARM data to directly infer the indirect effects of aerosols on climate. Further work is in progress with the 3-dimensional version of LLNL cloud resolving model to thoroughly explore the interactions between cloud dynamics and cloud microphysical details associated with aerosols, quantify the second indirect effect of aerosols on radiation fields, and address the associated uncertainties.

References

Beheng, KD. 1994. "A parameterization of warm cloud microphysical conversion processes." *Atmospheric Research* 33:193–206.

Berry, EX. 1967. "Cloud droplet growth by collection." *Journal of Atmospheric Science* 24:688-701.

Chen. C, and WR Cotton. 1987. "The physics of the marine stratoscumulus-capped mixed layer." *Journal of Atmospheric Science* 44:2951–2977.

Chin, H-NS. 1994. "The impact of the ice phase and radiation on a midlatitude squall line." *Journal of Atmospheric Science* 51:3320–3343.

Chin, H-NS, Q Fu, MM Bradley, and CR Molenkamp. 1995. "Modeling of a tropical squall line in two dimensions: Sensitivity to radiation and comparison with a midlatitude case." *Journal of Atmospheric Science* 52:3172–3193.

Chin, H-NS, and RB Wilhelmson. 1998. "Evolution and structure of tropical squall line elements within a moderate CAPE and strong low-level jet environment." *Journal of Atmospheric Science* 55:3089–3113.

Chuang, CC, JE Penner, KE Grant, JM Prospero, GH Rau, and K Kawamoto. 2002a. "Cloud susceptibility and the first aerosol indirect forcing: Sensitivity to black carbon and aerosol concentrations." *Journal of Geophysical Research* 107:4564.

Chuang, CC, D Bergman, J Dignon, and P Connell. 2002b. Final Report for LDRD Project "A New Era of Research in Aerosol/Cloud/Climate Interactions at LLNL," LDRD-UCRL-ID 146980. (http://www-r.llnl.gov/ibis/lof/documents/pdf/240899.pdf)

Chuang, CC. 2005. Implementation of the missing aerosol physics into LLNL IMPACT, LDRD-TR-209568. (http://www-r.llnl.gov/tid/lof/documents/pdf/316405.pdf)

Ferrare, RA, DD Turner, LA Heilman, O Dubovik, and W Feltz. 2001. "Raman lidar measurements of the aerosol extinction-to-backscatter ratio over the Southern Great Plains." *Journal of Geophysical Research* 106:20,333–20,347.

Fu, Q, and K-N Liou. 1993. "Parameterization of the radiative properties of cirrus clouds." *Journal of Atmospheric Science* 50:2008–2025.

Kessler, E. 1969. On the distribution and continuity of water substance in atmospheric circulation, Meteorological Monographs, Vol. 10, 84 pp. American Meteorological Society, Boston, Massachusetts.

Lohmann, U, and J Feichter. 1997. "Impact of sulfate aerosols on albedo and lifetime of clouds: A sensitivity study with the ECHAM4 GCM." *Journal of Geophysical Research* 102:13685–13700.

Rotman, DA, CS Atherton, DJ Bergmann, PJ Cameron-Smith, CC Chuang, PS Connell, JE Dignon, A Franz, KE Grant, DE Kinnison, CR Molenkamp, DD Proctor, and JR Tannahill. 2004. "IMPACT, the LLNL 3-D global atmospheric chemical transport model for the combined troposphere and stratosphere: model description and analysis of ozone and other trace gases." *Journal of Geophysical Research* 109.